

## N49: THE FIRST ROBUST DISCOVERY OF A RECOMBINING PLASMA IN AN EXTRA GALACTIC SUPERNOVA REMNANT

HIROYUKI UCHIDA<sup>1</sup>, KATSUJI KOYAMA<sup>1,2</sup>, HIROYA YAMAGUCHI<sup>3,4</sup>

*Draft version July 12, 2018*

### ABSTRACT

Recent discoveries of recombining plasmas (RPs) in supernova remnants (SNRs) have dramatically changed our understanding of SNR evolution. To date, a dozen of RP SNRs have been identified in the Galaxy. Here we present Suzaku deep observations of four SNRs in the Large Magellanic Cloud (LMC), N49, N49B, N23, and DEM L71, for accurate determination of their plasma state. Our uniform analysis reveals that only N49 is in the recombining state among them, which is the first robust discovery of a RP from an extra-galactic SNR. Given that RPs have been identified only in core-collapse SNRs, our result strongly suggests a massive star origin of this SNR. On the other hand, no clear evidence for a RP is confirmed in N23, from which detection of recombination lines and continua was previously claimed. Comparing the physical properties of the RP SNRs identified so far, we find that all of them are categorized into the “mixed-morphology” class and interacting with surrounding molecular clouds. This might be a key to solve formation mechanisms of the RPs.

*Subject headings:* ISM: abundances — ISM: individual (DEM L71, N23, N49, N49B) — supernova remnants — X-rays: ISM

### 1. INTRODUCTION

X-ray observations of supernova remnants (SNRs) allow us to make accurate measurements of plasma conditions and elemental abundances in the supernova (SN) ejecta, providing unique insights into the progenitor’s evolution and explosion as well as the dynamical evolution of the remnants themselves. The hot plasmas in X-ray-emitting SNRs are commonly in a state of non-equilibrium ionization (NEI), where the ionization degrees of heavy elements are inconsistent with those expected for a collisional ionization equilibrium (CIE) plasma with a certain electron temperature (e.g., Masai 1984). It had been widely believed for a long time that the SNR plasma is always in low-ionization, and slowly ionizing to achieve the CIE (hereafter “ionizing plasma”; IP). In fact, recent X-ray observations with sensitive satellites, like *Suzaku* (Mitsuda et al. 2007), have confirmed that the immediate post-shock gas in young SNRs indeed consists of extremely low ionized atoms together with hot electrons (e.g., Uchida et al. 2013; Yamaguchi et al. 2014b).

However, earlier *ASCA* observations had suggested presence of a recombining plasma (hereafter RP, where the atoms are overionized compared to the observed electron temperature) in a couple of SNRs, IC 443 and W49B (Kawasaki et al. 2002, 2005). The conclusive evidence for the RPs was revealed by later *Suzaku* observations that discovered enhanced radiative recombina-

tion continua (RRCs) in the X-ray spectra of these remnants (Yamaguchi et al. 2009; Ozawa et al. 2009). These results were followed by observational studies of other SNRs, leading to a significant increase in the number of RP SNRs. To date, RPs have been discovered from a dozen of SNRs, which means that the presence of RPs is no longer unusual or surprising.

The well-identified RP SNRs are all categorized into the so-called mixed-morphology (MM) class, defined by centrally-filled thermal X-ray emission with a synchrotron radio shell (Rho & Petre 1998). While more than 25% of the X-ray-detected Galactic SNRs are classified into this type (Jones et al. 1998), a physical process to form such characteristic morphology is still unclear. It is theoretically pointed out that dense ambient materials play an important role in the dynamical evolutions of MM SNRs (e.g., White & Long 1991; Petruk 2001). Notably, there is another prediction that the formation of RP can also be explained by interaction between the SN ejecta and dense materials surrounding the progenitor (e.g., Itoh & Masai 1989). Therefore, physical processes that create the mixed-morphology and RP seem related with each other.

It is noteworthy that the most RP SNRs identified so far were previously considered to have an IP or a nearly-CIE plasma (e.g., W44; Uchida et al. 2012). This implies that there are still a number of SNRs of which plasma state has been misclassified. Here, we present uniform analysis of high-quality data of MM SNRs (as well as typical shell-like SNRs simultaneously observed) in the Large Magellanic Cloud (LMC) obtained by the X-ray Imaging Spectrometer (XIS; Koyama et al. 2007) on board *Suzaku*, in order to search for a RP in these SNRs. The LMC is particularly suitable for such systematic study because of its low foreground extinction (Dickey & Lockman 1990) and its known distance of 50 kpc (Feast 1999); we use this distance throughout the paper.

Electronic address: uchida@cr.scphys.kyoto-u.ac.jp

<sup>1</sup> Department of Physics, Graduate School of Science, Kyoto University, Kitashirakawa Oiwake-cho, Sakyo-ku, Kyoto 606-8502, Japan

<sup>2</sup> Department of Earth and Space Science, Graduate School of Science, Osaka University, 1-1 Machikaneyama, Toyonaka, Osaka 560-0043, Japan

<sup>3</sup> NASA Goddard Space Flight Center, Code 662, Greenbelt, MD 20771, USA

<sup>4</sup> Department of Astronomy, University of Maryland, College Park, MD 20742, USA

In §2, we outline our observations and data reduction procedures. The results of spectral analysis of four LMC SNRs, N49, N23, N49B, and DEM L71 are presented in §3 — where we will show a new discovery of a RP from N49. We discuss our results in §4, and finally give conclusions and future prospect in §5. The errors quoted in text, tables, and figures are at the 90% confidence level unless otherwise stated.

## 2. OBSERVATIONS AND DATA REDUCTION

We observed two regions in the LMC aiming at the MM SNRs N23 and N49 during the *Suzaku* Cycle 8 phase. Detailed information of the observations is summarized in Table 1. In addition to the targeted sources, nearby SNRs DEM L71 and N49B are detected in each field of view (FoV) of the XIS. We analyzed their spectra as well, for comparison of the plasma states among the targets. Both DEM L71 and N49B are classified as standard shell-like SNRs (Hughes et al. 2003; Park et al. 2003b) from which a recombining plasma has never been observed to date.

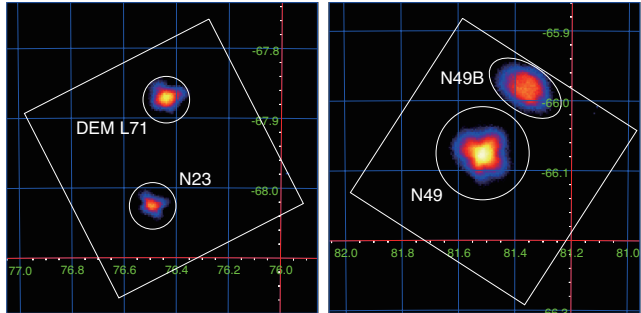
We analyzed data from three active CCDs; one is back-illuminated (XIS1) and the others are front-illuminated (XIS0 and XIS3), although only the merged and averaged front-illuminated (FI) CCD spectra are shown in Figures in the subsequent sections. We used HEASoft tools version 6.11 for the data reduction. The uncleaned data were reprocessed using the calibration database released in September 2011, and screened with the standard event selection criteria for cleaned events. The resulting effective exposures were 102 ks and 185 ks for the observations of N23 (with DEM L71) and N49 (with N49B), respectively.

## 3. ANALYSIS AND RESULTS

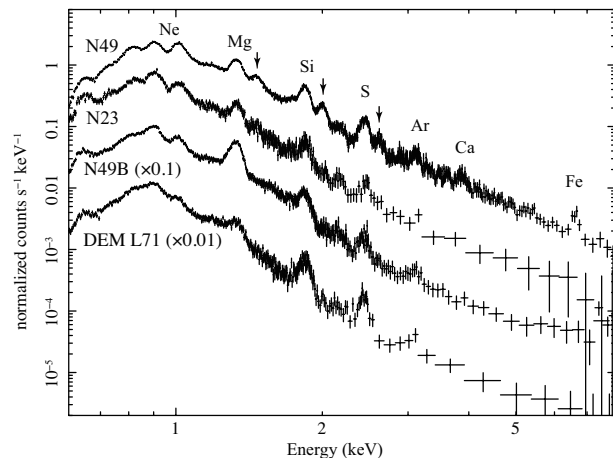
We show in Figure 1 the 0.6–10.0 keV images of the two observations after subtraction of non X-ray background (NXB) generated using *xisnabgen* (Tawa et al. 2008). Since the diameters of the SNRs ( $\lesssim 1'.5$ ; e.g., N49B; Park et al. 2003b) are smaller than the angular resolution of the X-Ray Telescopes of (XRTs; the half-power diameter ranges from  $1'.8$  to  $2'.3$ ), our analysis focuses on spectra from the entire SNRs. We extract the source spectra from the regions enclosed by the circles shown in Figure 1. The background spectra are taken from the entire FoV excluding the source regions as well as the CCD corners illuminated by the  $^{55}\text{Fe}$  calibration sources.

Figure 2 compares background-subtracted spectra of the four SNRs, showing that N49 is the brightest among them (with the count rate about  $\sim 10$  times higher than the others). Owing to the good energy resolution of the XIS, we clearly detect K-shell emission lines of Ar, Ca, and Fe from this remnant, for the first time. The spectrum of N49 exhibits strong Ly $\alpha$  lines of Mg, Si and S, whereas there is little or no signal of these lines from the other remnants. This indicates that the heavy elements in N49 are more highly ionized than those in the others. As our main goal is to identify a RP SNR(s), we first perform detailed spectral analysis of N49 (§3.1), which is followed by analysis of the other remnants (§3.2–3.4).

We use the SPEX software version 2.04.01 (Kaastra et al. 1996) for the spectral fitting by taking



**Figure 1.** Vignetting-corrected XIS FI images of the N23 (left) and N49 (right) regions in the 0.6–10.0 keV band with an equatorial coordinate grid. DEM L71 and N49B are also detected in the FoV of the XISs indicated by the solid squares.



**Figure 2.** XIS FI spectra of N49, N23, N49B and DEM L71, where the background spectra are subtracted. The spectra of N49B and DEM L71 are multiplied by factors of 0.1 and 0.01, respectively. The arrows represent the line centroids of Mg-Ly $\alpha$ , Si-Ly $\alpha$  and S-Ly $\alpha$ .

into account the detector and telescope responses (so-called “redistribution matrix” and “ancillary response”, respectively) generated by *xisrmfgen* and *xissarmfgen* (Ishisaki et al. 2007). The data around the neutral Si K-shell edge (1.77–1.83 keV) are ignored because of the poor accuracy in the response function at these energies<sup>5</sup>. During the analysis, we separately set absorption column densities in the Milky Way ( $N_{\text{H(MW)}}$ ) and the LMC ( $N_{\text{H(LMC)}}$ ). The former value is fixed to  $6 \times 10^{20} \text{ cm}^{-2}$  (Dickey & Lockman 1990). Elemental abundances of the latter component are fixed to the averages values of the LMC ( $\sim 0.3$  solar; Russell & Dopita 1992).

### 3.1. N49

N49 is one of the brightest SNRs in the LMC at the various wavelengths (e.g., Long et al. 1981; Dickel & Milne 1998). The radio continuum and H $\alpha$  emission exhibit a clear shell structure (Vancura et al. 1992; Dickel et al. 1995), whereas the X-ray image shows an irregular morphology brightest inside the radio shell in the southwest

<sup>5</sup> <http://heasarc.nasa.gov/docs/Suzaku/analysis/sical.html>

**Table 1**  
Observation logs.

Target	Obs. ID	Obs. Date	(R.A., Decl.) <sub>J2000</sub>	Exposure
N23 & DEM L71	807008010	2012 April 4	(76.45, -67.96)	102 ks
N49 & N49B	807007010	2012 May 9	(81.50, -66.08)	185 ks

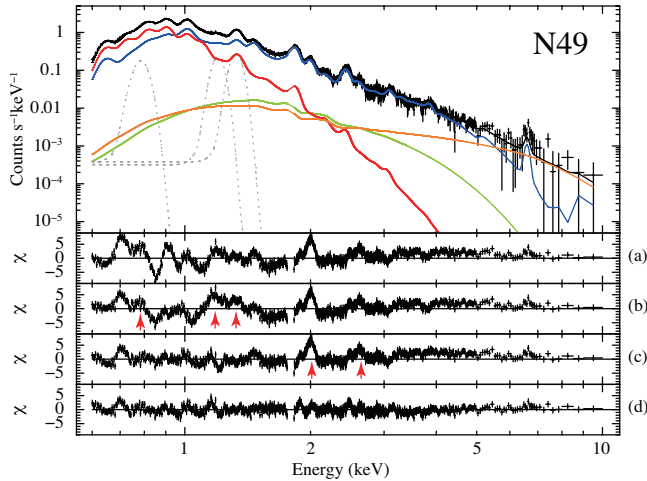


**Figure 3.** XIS FI spectrum of N49 (top panel). The best-fit model is overlaid with the black solid line. The solid blue and red lines represent the best-fit high- $kT_e$  (RP) and the low- $kT_e$  (IP) components, respectively. The orange and green lines show the power-law and the blackbody components for SGR 0526–66, respectively. The dotted lines show Gaussians for the Fe L emission missing from the plasma code we used. The residuals are shown in panel-(d). Panels (a), (b), and (c) represent the residuals from the models of single IP, two IP, and two IP plus Gaussians, respectively.

region (Park et al. 2012), which is the typical characteristic of a MM SNR. N49 is spatially overlapping with the soft gamma-ray repeater (SGR) 0526–66 (Cline et al. 1982), although the physical association between the SGR and SNR is under debate (Gaensler et al. 2001; Badenes et al. 2009). Using *Chandra* data, Park et al. (2012) revealed that the X-ray spectrum of SGR 0526–66 is best reproduced by a model consisting of a blackbody (BB) with  $kT_{\text{BB}} = 0.44 \pm 0.02$  keV and a power law (PL) with  $\Gamma = 2.50^{+0.11}_{-0.12}$ . Unfortunately, our *Suzaku* data do not spatially resolve the SGR from the SNR. We thus add the best-fit model by Park et al. (2012) to the model spectrum of N49, but allow its spectral parameters to vary within the reported statistical uncertainty. Since Park et al. (2012) found a significant long-term variability in the X-ray flux of the SGR, we also allow the fluxes of both BB and PL components to vary freely.

We first apply a single-component IP model where the initial ionization balance is dominated by the neutral state for all heavy elements. The free parameters are the electron temperature ( $kT_e$ ), ionization timescale ( $n_e t$ , where  $n_e$  and  $t$  are the electron number density and the elapsed time since the gas was shock heated), emission measure ( $EM = \int n_e n_H V$ ), and abundances of O, Ne, Mg, Si, S, Ar, Ca and Fe relative to the solar values of Anders & Grevesse (1989). The Ni abundance is linked to the value of Fe, while the abundances of the other elements are fixed to the LMC averages of Russell & Dopita

(1992). This model yields the best-fit electron temperature of  $\sim 0.6$  keV, but fails to reproduce the overall spectrum with an unacceptable  $\chi^2/\text{d.o.f.}$  of 4936/820. The residual is shown in panel (a) of Figure 3. The particularly large disagreement between the data and model is seen below  $\sim 1$  keV, implying presence of another plasma component with a lower temperature. Assuming that this component originates from a swept-up interstellar medium (ISM) that is dominant at the outermost region of the remnant (Park et al. 2003a, 2012), we added another IP component with the abundances fixed to the LMC mean values. Although this two-component model gives a slightly better fit ( $\chi^2/\text{d.o.f.} = 4297/817$ ), some line-like residuals still remain as shown in panel (b) of Figure 3. The residual at  $\sim 0.8$  keV, also observed in our previous studies of other objects (e.g., Uchida et al. 2013; Nakashima et al. 2013), is likely due to the well-known uncertainty in the emissivity ratio between the Fe XVIII L-shell emission of  $3s \rightarrow 2p$  and  $3d \rightarrow 2p$  (Gu et al. 2007). On the other hand, the residuals at  $\sim 1.2$  keV and  $\sim 1.3$  keV are caused by L-shell emission from high quantum numbers ( $n > 5$ ) missing from the plasma code SPEX (Brickhouse et al. 2000). We compensate for these lines by adding three Gaussians at these energies, and obtain the improved fit ( $\chi^2/\text{d.o.f.} = 2366/815$ ) with the best-fit  $kT_e$  of  $\sim 0.6$  keV and  $n_e t$  of  $\sim 10^{13} \text{ cm}^{-3} \text{ s}$  for the high- $kT_e$  component. The obtained ionization timescale indicates that this IP model actually represents a CIE plasma at the given temperature.

The fit left the largest residuals at 2.0 keV and 2.6 keV (see panel (c) of Figure 3), which correspond to the centroid energies of the Si Ly $\alpha$  and S Ly $\alpha$  emissions, respectively. This suggests that the average charge of these elements is higher than that expected in a 0.6-keV CIE plasma. Furthermore, a hump-like feature is found in the residual around 2.7 keV, indicating enhancement of the RRC of Si, as was observed in the other RP SNRs (e.g., IC 443; Yamaguchi et al. 2009). Therefore, we introduce a RP model (using an “NEIJ” model in SPEX<sup>6</sup>) for the high- $kT_e$  component. In addition to the parameters given in the IP model, the RP model has another free parameter  $kT_{\text{init}}$  of higher than  $kT_e$ , which describes a recombining history by  $n_e t$  in the  $kT_e$  plasma starting from the initial ionization temperature of  $kT_{\text{init}}$ . This model dramatically improves the fit ( $\chi^2/\text{d.o.f.} = 1270/813$ ), removing the large residuals above 2 keV as shown in the panel (d) of Figure 3. The best-fit model components and parameters are given in Figure 3 and Table 2, respectively.

Interestingly, the RP model reproduces the Fe K $\alpha$  emission at  $\sim 6.6$  keV as well, although free electrons in the 0.6-keV plasma are not energetic enough to excite

<sup>6</sup> See <http://www.sron.nl/files/HEA/SPEX/manuals/manual.pdf> for details.

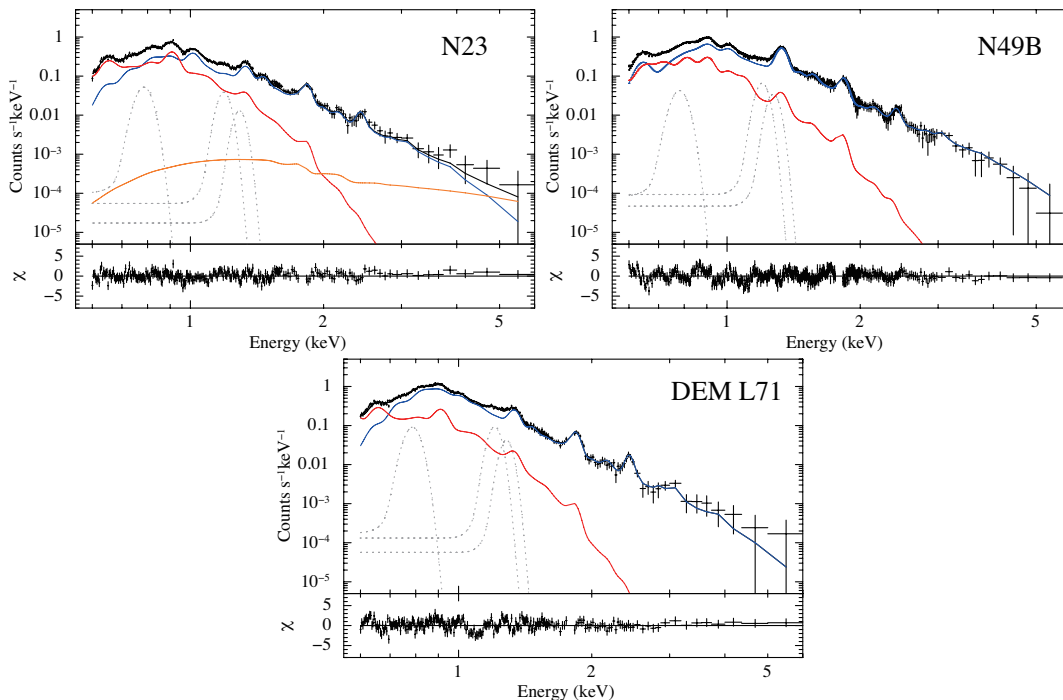


**Figure 4.** XIS FI spectra of N23 (upper left), N49B (upper right) and DEM L71 (bottom). The best-fit models are overlaid with the black solid lines. The solid blue and red lines represent the best-fit high- $kT_e$  and the low- $kT_e$  components, respectively. The dotted lines show Gaussians for the Fe L emission missing from the plasma code we used. The orange line in the model of N23 shows the power-law component for CXOU J050552.3–680141 (see text).

K-shell electrons of Fe. This indicates that the observed Fe  $K\alpha$  emission predominantly originates from cascade processes after the radiative recombination into the excited levels of He-like ions (i.e.,  $\text{Fe}^{25+} + e^- \rightarrow \text{Fe}^{24+*}$ ). We emphasize that this is why  $kT_{\text{init}}$  is constrained to the very high value ( $\gtrsim 10$  keV) so that a significant fraction of the Fe ions remains at the H-like state in the current plasma. It should also be noted that the observed centroid energy  $6629^{+31}_{-26}$  eV is consistent with the value expected from the best-fit RP model (6658 eV) but significantly lower than that for a typical CIE plasma at  $kT_e = 5\text{--}10$  keV ( $\sim 6680$  eV). This is another piece of evidence for the RP; the forbidden and intercombination lines are likely to be enhanced by the recombination processes.

### 3.2. N23

In the previous work using *XMM-Newton* MOS and RGS data, Broersen et al. (2011) claimed that the X-ray spectrum of N23 can be best reproduced by a two-component NEI model of which one of the components was a RP with  $kT_{\text{init}} = 3.0$  keV and  $kT_e = 0.18$  keV. We first fit the XIS spectrum fixing their best-fit parameters, but fail to reproduce the XIS spectrum ( $\chi^2/\text{d.o.f.} = 455/236$ ), leaving large residuals around the Ne-Ly $\alpha$  emission and the Fe XVII recombination edge at  $\sim 1.25$  keV. The fit is not improved even if we allow the abundances to vary. Therefore, we thaw the temperatures and ionization parameters (but restricting  $kT_{\text{init}}$  to be higher than  $kT_e$ ), obtaining a significantly better fit with  $\chi^2/\text{d.o.f.} = 224/234$  and  $n_e t > 10^{12}$  cm $^{-3}$  s for both components. This high  $n_e t$  value indicates that the plasmas are in nearly CIE independently from the initial

ionization population (otherwise ionizing). In fact, we are not able to constrain  $kT_{\text{init}}$  with this model. Finally, we apply an IP model consisting of a LMC-abundance component (for ISM) and a free-abundance component (for ejecta), and obtain a slightly better fit ( $\chi^2/\text{d.o.f.} = 218/234$ ) than the RP (or CIE) model. The best-fit parameters and models are given in Table 2 and Figure 4, respectively. During the analysis, we fix the spectral shape and flux of the faint X-ray compact source CXOU J050552.3–680141 associated with N23 to the reported values of Hayato et al. (2006), although its contribution is negligible at  $\lesssim 3$  keV (see Figure 4).

### 3.3. N49B

N49B is a typical shell-like SNR containing no X-ray point-like source within the SNR shell (Park et al. 2003b). We fit the XIS spectrum with the same two-component IP model applied to N49, obtaining the best-fit results given in Table 2. The  $n_e t$  value for the ejecta component ( $\sim 8 \times 10^{10}$  cm $^{-3}$  s) is the lowest among the SNRs studied in this work. We reveal that the abundance of Mg is significantly higher than those of the other elements (e.g., Mg/O  $\sim 2.0$ , Mg/Ne  $\sim 2.8$ , Mg/Si  $\sim 3.6$ ). Park et al. (2003b) previously found “Mg-rich” ejecta near the center of the remnant. Our result shows that the Mg enrichment is confirmed even in the integrated spectrum from the entire SNR. We find no evidence for a RP; if  $kT_{\text{init}} > kT_e$  is assumed, the model clearly fail to reproduce the spectrum with  $\chi^2/\text{d.o.f.} = 1582/426$ . Therefore, we conclude that this SNR is dominated by IPs.

### 3.4. DEM L71

**Table 2**  
Best fit parameters

Component	Parameter	N49	N23	N49B	DEM L71
Absorption	$N_{\text{H(LMC)}} (\times 10^{21} \text{ cm}^{-2})$	$3.51^{+0.01}_{-0.04}$	$2.13 \pm 0.05$	$2.30^{+0.01}_{-0.06}$	$3.70^{+0.30}_{-0.50}$
	$N_{\text{H(MW)}} (\times 10^{21} \text{ cm}^{-2})$	0.6 (fixed)	0.6 (fixed)	0.6 (fixed)	0.6 (fixed)
ISM	$kT_e$ (keV)	$0.30 \pm 0.01$	$0.17 \pm 0.01$	$0.21 \pm 0.01$	$0.16 \pm 0.01$
	$n_{et} (\times 10^{11} \text{ cm}^{-3} \text{ s})$	$3.49^{+0.09}_{-0.26}$	> 10	$1.23^{+0.09}_{-0.07}$	> 10
	$EM (\times 10^{58} \text{ cm}^{-3})$	$3.54^{+0.03}_{-0.01}$	$17.6 \pm 0.3$	$6.0 \pm 0.9$	$19^{+5}_{-4}$
Ejecta	$kT_e$ (keV)	$0.62 \pm 0.01$	$0.61 \pm 0.01$	$0.79 \pm 0.01$	$0.69 \pm 0.01$
	$kT_{\text{init}}$ (keV)	$11 \pm 1$	0.01 (fixed)	0.01 (fixed)	0.01 (fixed)
	$n_{et} (\times 10^{11} \text{ cm}^{-3} \text{ s})$	$7.00^{+0.44}_{-0.02}$	$5.08^{+0.42}_{-0.37}$	$0.84 \pm 0.01$	$1.77 \pm 0.07$
	O	$1.52^{+0.04}_{-0.03}$	$3.5 \pm 0.2$	$0.63^{+0.03}_{-0.02}$	$0.30^{+0.05}_{-0.04}$
	Ne	$0.98^{+0.03}_{-0.02}$	$1.25 \pm 0.07$	$0.45 \pm 0.01$	$0.25 \pm 0.02$
	Mg	$0.82 \pm 0.02$	$1.16 \pm 0.07$	$1.24 \pm 0.02$	$0.62 \pm 0.03$
	Si	$1.32^{+0.05}_{-0.02}$	$1.2 \pm 0.4$	$0.34 \pm 0.02$	$0.48 \pm 0.04$
	S	$1.46^{+0.03}_{-0.11}$	$1.25 \pm 0.08$	$0.50 \pm 0.08$	$1.0 \pm 0.2$
	Ar	$1.3^{+0.1}_{-0.5}$	< 3.1	$0.7 \pm 0.6$	$1.5^{+3.1}_{-0.3}$
	Ca	$1.5^{+0.2}_{-0.9}$	(=Ar)	(=Ar)	(=Ar)
Fe (=Ni)	$0.24 \pm 0.01$	$0.46 \pm 0.02$	$0.35 \pm 0.01$	$0.62 \pm 0.01$	
	$EM (\times 10^{58} \text{ cm}^{-3})$	$1.73 \pm 0.01$	$0.62 \pm 0.01$	$0.79 \pm 0.01$	$1.36 \pm 0.01$
	$\chi^2/\text{d.o.f.}$	1270/813	218/234	659/423	291/229

DEM L71 is a middle-aged shell-like SNR, where a double-shock morphology was observed by *Chandra* observations (Hughes et al. 2003), suggesting the presence of both reverse-shocked ejecta and swept-up ISM. Hughes et al. (2003) also revealed that the X-ray spectra from the interior regions are dominated by strong Fe L emission. Similarly to the spectral analysis of N49B, we fit the XIS spectrum of DEM L71 with a two-component IP model consisting of a low- $kT_e$  ISM and a high- $kT_e$  ejecta. The fit is acceptable with  $\chi^2/\text{d.o.f.}$  of 291/229 as is given in Table 2. The Fe abundance is highest among the four SNRs, consistent with the previous studies (e.g., Hughes et al. 1998, 2003) where the Type Ia origin of this SNR was suggested. If we assume  $kT_{\text{init}} > kT_e$ , an unacceptable fit ( $\chi^2/\text{d.o.f.} = 399/228$ ) is obtained, ruling out a RP scenario for this remnant.

#### 4. DISCUSSION

##### 4.1. Plasma Conditions in the Observed SNRs

We have systematically analyzed X-ray spectra from the four LMC SNRs (N49, N23, N49B, and DEM L71), and revealed the robust evidence for overionization in N49 — this is the first discovery of a RP from an extragalactic SNR. The other SNRs, including N23 from which presence of a RP was previously reported (Broersen et al. 2011), can be fairly well characterized by an IP or a nearly-CIE plasma.

The previous claim of the recombining state in N23 was based on the enhanced  $G$ -ratio of the O VII lines measured using the *XMM-Newton* RGS. Although Broersen et al. (2011) claimed that the broadband spectrum of the *XMM-Newton* MOS can also be reproduced by a RP model, their best-fit model is clearly ruled out by our analysis of the XIS spectrum with better photon statistics. Since our analysis excluded the O VII emission, it is still possible that the swept-up ISM (low- $kT_e$  component) is partially recombining. We note, however, that there are several other processes that can enhance the  $G$ -ratio: resonance scattering and charge exchange.

Notably, a similar  $G$ -ratio enhancement in the O VII lines was observed in DEM L71, and was indeed interpreted to be a consequence of the resonance scattering (van der Heyden et al. 2003). Since the charge exchange process seems to work in some evolved SNRs (e.g., Puppis A; Katsuda et al. 2012), this process may also be responsible for the high  $G$ -ratio observed in N23.

##### 4.2. Origin of the Recombining Plasma

We summarize the characteristics of the four SNRs studied in this work in Table 3. Only N49 is interacting with dense clouds identified by the CO (Banas et al. 1997) and H $\alpha$  (Melnik & Copetti 2013) observations. Given that similar cloud interaction is observed in most SNRs from which the presence of a RP has been confirmed (e.g., W49B; Ozawa et al. 2009), thermal conduction into surrounding clouds might play an important role in forming the RP (see Zhou et al. 2011, for a discussion). In this scenario, there should be a spatial correlation between the electron temperature of the SNR plasma and the cloud density. Future deep observations of N49 with better spatial resolution are necessary to assess this possibility.

An alternative is that the adiabatic expansion of the SNR had caused a rapid cooling of electrons and the resulting recombining state of the plasma. In this scenario, the SN ejecta should interact with a dense circumstellar matter (CSM) in the early phase of the SNR evolution, and the highly ionized ejecta and CSM expand drastically after the SNR blast wave breaks out to the low-density ISM (Itoh & Masai 1989). Therefore, the ionization timescale ( $n_{et}$ ) in this scenario is characterized by the elapsed time and the density evolution history since the break out took place. To evaluate the possibility of this scenario, we estimate the electron density in the present RP of N49 using the derived  $EM (= n_e n_{\text{H}} V)$ . Since the plasma density is known to be highly inhomogeneous in this remnant (Park et al. 2012), we analyze archival *Chandra* data of N49 to investigate the surface

**Table 3**  
Summary of the Four LMC SNRs Studied in This Work

SNR	RP	Age ( $10^4$ yr)	SN Type	Morphology	Cloud Interaction	References
N49	Yes	0.4–0.5	Core-collapse	MM	Yes (CO and H $\alpha$ )	this work, 1, 2, 3
N23	No	0.4	Core-collapse	MM	No	2, 4
N49B	No	1.09	Core-collapse	Shell	No	5
DEM L71	No	0.4–0.5	Ia	Shell	No	6, 7, 8

**References.** — (1) Park et al. 2012; (2) Banas et al. 1997; (3) Melnik & Copetti 2013; (4) Broersen et al. 2011; (5) Park et al. 2003b; (6) Ghavamian et al. 2003; (7) Hughes et al. 1998; (8) Hughes et al. 2003.

brightness profile. We find that  $\sim 50\%$  of the photon flux in the Si band (1.7–2.1 keV) is coming from the brightest southeast region (approximately a  $0.4 \times 0.25 \times 0.25$  ellipsoid), and the other  $\sim 50\%$  is from the remaining faint region in the entire SNR (a sphere with a radius of 0.6). Therefore, the volumes and the electron densities are estimated to be  $9.6 \times 10^{57} \text{ cm}^3$  and  $1.0 \text{ cm}^{-3}$  for the bright region, and  $7.3 \times 10^{58} \text{ cm}^3$  and  $0.38 \text{ cm}^{-3}$  for the faint region, at a distance of 50 kpc. If we simply divide the best-fit  $n_e t$  in the ejecta component ( $7.0 \times 10^{11} \text{ cm}^{-3} \text{ s}$ ) by the derived electron density, we obtain plasma ages of 22–58 kyr, more than a few times larger than the dynamical age of N49 ( $\sim 4800$  yr; Park et al. 2012). This is not surprising because the plasma must have had a higher electron density in the past. Yamaguchi et al. (2012) also obtained a similar result from the *Suzaku* observation of IC 443, where the plasma age estimate ( $\sim 11$  kyr) is significantly higher than the SNR age of  $\sim 4000$  yr (Troja et al. 2008).

In Table 4, we summarize physical properties of the RP SNRs identified so far. While the estimated ages are roughly correlated with  $kT_e$ , the values of  $n_e t$  show no clear trend. This may be partly due to a technical reason that the parameter  $n_e t$  is coupled to that of  $kT_{\text{init}}$  in the spectral fitting. Nevertheless, Table 4 shows that the  $n_e t$  values exceed  $\sim 10^{11} \text{ cm}^{-3} \text{ s}$  in all SNRs, implying that the overionization did *not* start from the last few hundred years, but from the early epoch in the SNR. This fact likely favors the adiabatic cooling scenario for the most RP SNRs.

#### 4.3. Progenitor of N49 and SGR 0526–66

The SN type of N49 has been controversial. Park et al. (2012) suggested a Type Ia origin based on the Si/S abundance ratio in the ejecta measured by the *Chandra* data. On the other hand, the environment of N49, i.e., a nearby OB association (Chu & Kennicutt 1988) and young stellar clusters (Klose et al. 2004), are more common in core-collapse SNRs. A recent systematic study of Fe K emissions in young and middle-aged SNRs also agrees on its core-collapse origin (Yamaguchi et al. 2014a). Given that a RP has never been observed in a Type Ia SNR, our results strongly support a core-collapse scenario for this SNR. It should also be noted that the formation of a RP needs dense CSM, which is only made by a massive progenitor with a significant mass loss rate (Moriya 2012; Shimizu et al. 2012). The total mass of the RP component is roughly estimated to be  $\sim 26 M_\odot$  using the density and emitting volume derived in §4.2, which is in marginal agreement with the progenitor mass of 12.5–21.5  $M_\odot$  constrained from the local star forma-

tion history around N49 (Badenes et al. 2009).

Since the core-collapse origin is strongly suggested for N49, the compact object SGR 0526–66, which is known to be a magnetar candidate (e.g., Park et al. 2012), might be associated with the SNR. The large distance between SGR 0526–66 and the geometric center of N49 requires a high kick velocity ( $\sim 1100 \text{ km s}^{-1}$ ) for the SGR at the SNR age of  $\sim 4800$  yr, and hence Park et al. (2012) argued against the physical association between these objects. However, the theoretical prediction is that a magnetorotational core-collapse SN explodes asymmetrically with bipolar jets and produces a magnetar with a large kick velocity up to  $\sim 1000 \text{ km s}^{-1}$  (Sawai et al. 2008). Moreover, there are several compact objects located extremely off-center from the associated RP SNRs. For instance, IGR J11014–6103 is located outside the shell of MSH 11-61A. Pavan et al. (2014) indicated that this neutron star is escaping from MSH 11-61A at a velocity exceeding  $1000 \text{ km s}^{-1}$ . Also, PSR 1758–23 is known as a “runaway pulsar” which might be physically associated with W28 (Frail et al. 1993). Two other compact objects, CXOU J171419.8–383023 in CTB 37A (Aharonian et al. 2008a) and XMMU J061804.3+222732 in IC 443 (Olbert et al. 2001), are also found far from the geometric center of their host SNRs. Taking these facts into consideration, we propose that SGR 0526–66 is the plausible candidate of the compact remnant of N49.

## 5. CONCLUSIONS

We have shown the clear evidence for the RP in the SNR N49, which is the first report of the robust detection of a RP from an extra-galactic SNR achieved by the high sensitivity and the good energy resolution of the XIS on board *Suzaku*. The other SNRs, including N23 where presence of a RP was previously claimed (Broersen et al. 2011), can be well characterized by an IP or a nearly-CIE plasma. A future observation of N49 using high-resolution X-ray spectrometers, like *ASTRO-H* (Takahashi et al. 2014), is highly encouraged; our *Suzaku* result predicts the detection of the Fe RRC as well as the enhanced forbidden lines due to the recombination processes (see §3.1). We also emphasize the importance of a systematic study of the RP SNRs, which will help us understand physical processes responsible for the formation of the RPs in more details.

The authors thank to Dr. T. G. Tsuru for a careful reading of our manuscript. This work is supported by JSPS KAKENHI Grand Numbers 26800102 (H.U.) and 2450229 (K.K.).

*Facilities:* *Suzaku* (XIS).

**Table 4**  
List of the RP SNRs in the Order of Increasing Electron Temperature

SNR	Age ( $10^4$ yr)	$kT_{\text{init}}$ (keV)	$kT_e$ (keV)	$n_{e,t}$ ( $10^{11}$ cm $^{-3}$ s)	Cloud Interaction	Compact Object	References
G359.1–0.5	> 1	$0.87^{+0.15}_{-0.11}$	$0.29 \pm 0.02$	< 4.42	Yes	...	1, 2, 24
G346.6–0.2	...	5 (fixed)	$0.30^{+0.03}_{-0.01}$	$4.8^{+0.1}_{-0.4}$	Yes	...	3, 25
W28	~ 4	3 (fixed)	$0.40^{+0.02}_{-0.03}$	6.31	Yes	PSR 1758–23	4, 5, 6, 24
W44	~ 2	$1.07^{+0.08}_{-0.06}$	$0.48 \pm 0.02$	$6.76 \pm 0.5$	Yes	PSR B1853+01	7, 8, 9, 24
CTB 37A	~ 1	5 (fixed)	$0.49^{+0.09}_{-0.06}$	$13^{+3}_{-1}$	Yes	CXOU J171419.8–383023	10, 11, 12, 24
3C391	...	$1.8^{+1.6}_{-0.6}$	$0.495 \pm 0.015$	$14.0^{+1.5}_{-2.2}$	Yes	...	13, 24
MSH 11-61A	1–2	5 (fixed)	$0.513^{+0.004}_{-0.003}$	$12.2 \pm 0.4$	Possible	IGR J11014-6103	14, 15, 16, 26
N49	0.4–0.5	$11 \pm 1$	$0.62 \pm 0.01$	$7.00^{+0.44}_{-0.02}$	Yes	SGR 0526–66	this work, 17
IC 443	~ 0.4	10 (fixed)	$0.65 \pm 0.04$	$9.8 \pm 1.1$	Yes	XMMU J061804.3+222732	18, 19, 20, 21, 24
W49B	~ 0.4	...	$1.52^{+0.01}_{-0.02}$	...	Yes	...	22, 23, 27

**Note.** — The plasma parameters for IC 443 and W49B were determined only from a high-energy band around Fe-K lines (e.g., Ohnishi et al. 2014; Ozawa et al. 2009), while those for the other SNRs were determined from intermediate-mass elements.

**References.** — (1) Aharonian et al. 2008b; (2) Ohnishi et al. 2011; (3) Yamauchi et al. 2013; (4) Rho & Borkowski 2002; (5) Sawada & Koyama 2012; (6) “runaway” Pulsar; Frail et al. 1993; (7) Cox et al. 1999; (8) Uchida et al. 2012; (9) Pulsar plus Pulsar Wind Nebula; Petre et al. 2002; (10) Yamauchi et al. 2014; (11) Wolszczan et al. 1991; (12) Pulsar Wind Nebula candidate; Aharonian et al. 2008a; (13) Sato et al. 2014; (14) Slane et al. 2002; (15) Kamitsukasa et al. 2015; (16) Pulsar plus Pulsar Wind Nebula; Pavan et al. 2014; (17) Park et al. 2012; (18) Lee et al. 2008; (19) Yamaguchi et al. 2009; (20) Ohnishi et al. 2014; (21) Neutronstar plus Synchrotron Nebula; Olbert et al. 2001; (22) Hwang et al. 2000; (23) Ozawa et al. 2009; (24) Hewitt et al. 2008; (25) Koralesky et al. 1998; (26) Filipović et al. 2005; (27) Keohane et al. 2007.

## REFERENCES

- Aharonian, F., Akhperjanian, A. G., Barres de Almeida, U., et al. 2008a, *A&A*, 490, 685  
— 2008b, *A&A*, 483, 509  
Anders, E., & Grevesse, N. 1989, *Geochim. Cosmochim. Acta*, 53, 197  
Badenes, C., Harris, J., Zaritsky, D., & Prieto, J. L. 2009, *ApJ*, 700, 727  
Banas, K. R., Hughes, J. P., Bronfman, L., & Nyman, L.-Å. 1997, *ApJ*, 480, 607  
Brickhouse, N. S., Dupree, A. K., Edgar, R. J., et al. 2000, *ApJ*, 530, 387  
Broersen, S., Vink, J., Kaastra, J., & Raymond, J. 2011, *A&A*, 535, A11  
Chu, Y.-H., & Kennicutt, Jr., R. C. 1988, *AJ*, 96, 1874  
Cline, T. L., Desai, U. D., Teegarden, B. J., et al. 1982, *ApJ*, 255, L45  
Cox, D. P., Shelton, R. L., Maciejewski, W., et al. 1999, *ApJ*, 524, 179  
Dickel, J. R., & Milne, D. K. 1998, *AJ*, 115, 1057  
Dickel, J. R., Chu, Y.-H., Gelino, C., et al. 1995, *ApJ*, 448, 623  
Dickey, J. M., & Lockman, F. J. 1990, *ARA&A*, 28, 215  
Feast, M. 1999, *PASP*, 111, 775  
Filipović, M. D., Payne, J. L., Reid, W., et al. 2005, *MNRAS*, 364, 217  
Frail, D. A., Kulkarni, S. R., & Vasisht, G. 1993, *Nature*, 365, 136  
Gaensler, B. M., Slane, P. O., Gotthelf, E. V., & Vasisht, G. 2001, *ApJ*, 559, 963  
Ghavamian, P., Rakowski, C. E., Hughes, J. P., & Williams, T. B. 2003, *ApJ*, 590, 833  
Gu, M. F., Chen, H., Brown, G. V., Beiersdorfer, P., & Kahn, S. M. 2007, *ApJ*, 670, 1504  
Hayato, A., Bamba, A., Tamagawa, T., & Kawabata, K. 2006, *ApJ*, 653, 280  
Hewitt, J. W., Yusef-Zadeh, F., & Wardle, M. 2008, *ApJ*, 683, 189  
Hughes, J. P., Ghavamian, P., Rakowski, C. E., & Slane, P. O. 2003, *ApJ*, 582, L95  
Hughes, J. P., Hayashi, I., & Koyama, K. 1998, *ApJ*, 505, 732  
Hwang, U., Petre, R., & Hughes, J. P. 2000, *ApJ*, 532, 970  
Ishisaki, Y., Maeda, Y., Fujimoto, R., et al. 2007, *PASJ*, 59, 113  
Itoh, H., & Masai, K. 1989, *MNRAS*, 236, 885  
Jones, T. W., Rudnick, L., Jun, B.-I., et al. 1998, *PASP*, 110, 125  
Kaastra, J. S., Mewe, R., & Nieuwenhuijzen, H. 1996, in *UV and X-ray Spectroscopy of Astrophysical and Laboratory Plasmas*, ed. K. Yamashita & T. Watanabe, 411–414  
Kamitsukasa, F., Koyama, K., Uchida, H., et al. 2015, *PASJ*, 67, 16  
Katsuda, S., Tsunemi, H., Mori, K., et al. 2012, *ApJ*, 756, 49  
Kawasaki, M., Ozaki, M., Nagase, F., Inoue, H., & Petre, R. 2005, *ApJ*, 631, 935  
Kawasaki, M. T., Ozaki, M., Nagase, F., et al. 2002, *ApJ*, 572, 897  
Keohane, J. W., Reach, W. T., Rho, J., & Jarrett, T. H. 2007, *ApJ*, 654, 938  
Klose, S., Henden, A. A., Geppert, U., et al. 2004, *ApJ*, 609, L13  
Koralesky, B., Frail, D. A., Goss, W. M., Claussen, M. J., & Green, A. J. 1998, *AJ*, 116, 1323  
Koyama, K., Tsunemi, H., Dotani, T., et al. 2007, *PASJ*, 59, 23  
Lee, J.-J., Koo, B.-C., Yun, M. S., et al. 2008, *AJ*, 135, 796  
Long, K. S., Helfand, D. J., & Grabelsky, D. A. 1981, *ApJ*, 248, 925  
Masai, K. 1984, *Ap&SS*, 98, 367  
Melnik, I. A. C., & Copetti, M. V. F. 2013, *A&A*, 553, A104  
Mitsuda, K., Bautz, M., Inoue, H., et al. 2007, *PASJ*, 59, 1  
Moriya, T. J. 2012, *ApJ*, 750, L13  
Nakashima, S., Nobukawa, M., Uchida, H., et al. 2013, *ApJ*, 773, 20  
Ohnishi, T., Koyama, K., Tsuru, T. G., et al. 2011, *PASJ*, 63, 527  
Ohnishi, T., Uchida, H., Tsuru, T. G., et al. 2014, *ApJ*, 784, 74  
Olbert, C. M., Clearfield, C. R., Williams, N. E., Keohane, J. W., & Frail, D. A. 2001, *ApJ*, 554, L205  
Ozawa, M., Koyama, K., Yamaguchi, H., Masai, K., & Tamagawa, T. 2009, *ApJ*, 706, L71  
Park, S., Burrows, D. N., Garmire, G. P., et al. 2003a, *ApJ*, 586, 210  
Park, S., Hughes, J. P., Slane, P. O., et al. 2012, *ApJ*, 748, 117  
— 2003b, *ApJ*, 592, L41  
Pavan, L., Bordas, P., Pühlhofer, G., et al. 2014, *A&A*, 562, A122  
Petre, R., Kuntz, K. D., & Shelton, R. L. 2002, *ApJ*, 579, 404  
Petruk, O. 2001, *A&A*, 371, 267  
Rho, J., & Borkowski, K. J. 2002, *ApJ*, 575, 201  
Rho, J., & Petre, R. 1998, *ApJ*, 503, L167  
Russell, S. C., & Dopita, M. A. 1992, *ApJ*, 384, 508  
Sato, T., Koyama, K., Takahashi, T., Odaka, H., & Nakashima, S. 2014, *PASJ*, 66, 124  
Sawada, M., & Koyama, K. 2012, *PASJ*, 64, 81  
Sawai, H., Kotake, K., & Yamada, S. 2008, *ApJ*, 672, 465  
Shimizu, T., Masai, K., & Koyama, K. 2012, *PASJ*, 64, 24  
Slane, P., Smith, R. K., Hughes, J. P., & Petre, R. 2002, *ApJ*, 564, 284  
Takahashi, T., Mitsuda, K., Kelley, R., et al. 2014, in *Society of Photo-Optical Instrumentation Engineers (SPIE) Conference Series*, Vol. 9144, Society of Photo-Optical Instrumentation Engineers (SPIE) Conference Series, 25  
Tawa, N., Hayashida, K., Nagai, M., et al. 2008, *PASJ*, 60, 11  
Troja, E., Bocchino, F., Miceli, M., & Reale, F. 2008, *A&A*, 485, 777  
Uchida, H., Yamaguchi, H., & Koyama, K. 2013, *ApJ*, 771, 56

- Uchida, H., Koyama, K., Yamaguchi, H., et al. 2012, PASJ, 64, 141
- van der Heyden, K. J., Bleeker, J. A. M., Kaastra, J. S., & Vink, J. 2003, A&A, 406, 141
- Vancura, O., Blair, W. P., Long, K. S., & Raymond, J. C. 1992, ApJ, 394, 158
- White, R. L., & Long, K. S. 1991, ApJ, 373, 543
- Wolszczan, A., Cordes, J. M., & Dewey, R. J. 1991, ApJ, 372, L99
- Yamaguchi, H., Ozawa, M., Koyama, K., et al. 2009, ApJ, 705, L6
- Yamaguchi, H., Ozawa, M., & Ohnishi, T. 2012, Advances in Space Research, 49, 451
- Yamaguchi, H., Badenes, C., Petre, R., et al. 2014a, ApJ, 785, L27
- Yamaguchi, H., Eriksen, K. A., Badenes, C., et al. 2014b, ApJ, 780, 136
- Yamauchi, S., Minami, S., Ota, N., & Koyama, K. 2014, PASJ, 66, 2
- Yamauchi, S., Nobukawa, M., Koyama, K., & Yonemori, M. 2013, PASJ, 65, 6
- Zhou, X., Miceli, M., Bocchino, F., Orlando, S., & Chen, Y. 2011, MNRAS, 415, 244